

**Anisotropically Branched Metal Nanostructures**

Journal:	<i>Chemical Society Reviews</i>
Manuscript ID:	CS-TRV-03-2015-000213.R1
Article Type:	Tutorial Review
Date Submitted by the Author:	27-Apr-2015
Complete List of Authors:	Ye, Enyi; Institute of Materials Research and Engineering, Regulacio, Michelle; Institute of Materials Research and Engineering, Zhang, Shuang-Yuan; Institute of Materials Research and Engineering, Loh, Xian Jun; Institute of Materials Research and Engineering (IMRE), Han, Mingyong; Institute of Materials Research and Engineering,

Anisotropically Branched Metal Nanostructures

Enyi Ye,⁺ Michelle D. Regulacio,⁺ Shuang-Yuan Zhang, Xian Jun Loh, Ming-Yong Han*

Institute of Materials Research and Engineering (IMRE), Agency for Science, Technology and Research (A*STAR), 3 Research Link, Singapore 117602

⁺These authors contributed equally to this work.

*E-mail: my-han@imre.a-star.edu.sg

Abstract:

Metal nanostructures display a multitude of technologically useful properties that can be tailored through fine-tuning of certain parameters, such as size, shape and composition. In many cases, the shape or morphology of metal nanostructures plays the most crucial role in the determination of their properties and their suitability in specific applications. In this tutorial review, we provide a summary of recent research that centers on metal nanostructures having anisotropically branched morphologies. The branched structural features that are exhibited by these materials endow them with unique properties that can be utilized in many important applications. The formation of branched architectures can be achieved in solution through a variety of synthetic strategies, four of which are highlighted in this review and these are: (1) seedless growth, (2) seeded growth, (3) templated growth, and (4) chemical etching. The usefulness of these anisotropically branched metal nanostructures in the areas of plasmonics, catalysis and biomedicine is also presented.

Key learning points

- (1) Importance of shape control in tuning the properties of metal nanostructures
- (2) Factors that influence the shape-controlled synthesis of metal nanostructures
- (3) Different solution-based routes to anisotropic branching of metal nanostructures
- (4) Properties and applications of anisotropically branched metal nanostructures

1. Introduction

In the nanometer-size regime, metals display distinctive and fascinating properties that render them useful in a broad range of applications that span across multiple areas of research. As with other nanoscale materials, the size and shape of nanostructured metals are two crucial parameters that can be tailored to modify their properties and meet specific functions for different applications. While the nanocrystal size determines the surface area and the percentage of surface atoms, the shape or morphology governs the surface structure (i.e., the arrangement of atoms on the surface) and the surface atom composition. In many cases, shape offers better versatility than size in tuning the properties of metal nanostructures mainly because different nanocrystal facets exhibit different physical and chemical properties. For instance, it has been shown that the catalytic activity and selectivity of the nanostructures of Pt and Pd are strongly dependent on the type of facets exposed on the surface.^{1, 2} This type of structural sensitivity has received significant interest and has been applied in many important catalytic reactions, such as oxygen reduction reaction and formic acid oxidation. Meanwhile, it has been established that altering the geometry can dramatically change the surface plasmon resonance (SPR) characteristics of nanostructured metals.³ Enhanced plasmonic sensitivity has been particularly observed for Au nanostructures with anisotropic shapes, allowing their use in surface-enhanced Raman scattering (SERS), sensing, imaging, and photothermal therapy.³⁻⁵ Shape variation has also been reported to result in different bactericidal properties of Ag nanostructures against *Escherichia coli*, and this is due to the shape-dependent interaction of nanostructured Ag with the gram-negative organism.⁶ As different applications demand nanostructures of specific metals with particular morphologies, the synthesis of various metal nanostructures with controllable shapes has become the target of extensive research in many laboratories worldwide.

Nanoscale metals with specific morphologies can be conveniently prepared as colloids through wet-chemical synthetic methods (i.e., solution-based routes). The earliest documented work on the colloidal preparation of metal nanostructures dates back to the mid-19th century, when Michael Faraday produced spherical-shaped Au nanoparticles by reducing gold chloride with phosphorus in water.⁷ In the following century, a number of synthetic protocols have been developed for preparing colloidal metal nanostructures of varying shapes, but it is only within the last decade that the construction of high-quality metal nanostructures with amazingly complex geometries has been achieved. In accordance to Wulff's theorem, a nanocrystalline metal with a face-centered cubic (*fcc*) lattice adopts the truncated octahedron geometry (known as Wulff

polyhedron) as its equilibrium shape when in an inert gas or vacuum.^{8, 9} This, however, is not usually observed when nanocrystals are grown in solution due to a number of factors, such as the presence of capping agents that alters the surface energies of different nanocrystal facets and the inclusion of twin defects, which leads to shapes with a total free energy that is lower than that of the Wulff polyhedron. For this reason, the solution-based approach to nanocrystal synthesis has emerged as a powerful and versatile tool for preparing metal nanostructures with a wide variety of shapes that range from simple geometries like rods, cubes, and plates, to more complicated morphologies, such as cages, hollow structures, and highly branched architectures.⁹⁻¹²

In this tutorial review, particular attention is drawn to metal nanostructures with anisotropically branched morphologies. The branched structural features that are unique to this class of metal nanostructures have been proven to be beneficial in the enhancement of properties that can be exploited in a plethora of technological applications. Fig. 1 provides a pictorial representation that summarizes the four main strategies that have been used to achieve anisotropic branching of metal nanostructures in solution. These colloidal-based synthetic routes are described fully in Section 2. Meanwhile, Section 3 highlights the novel characteristics of anisotropically branched metal nanostructures and their applications in the areas of catalysis, plasmonics and biomedicine. Lastly, the main conclusions and outlook are presented in the final section.

2. Strategies for anisotropic branching of metal nanostructures

It is well known that the appropriate choice of synthetic method and experimental conditions is pivotal to achieving a fine degree of control over the size and shape of nanostructured materials. In creating branched metal nanostructures, several synthetic approaches have been reported and the mechanism of branch formation varies depending on the approach. In this section, we present the different wet-chemistry-based synthetic protocols that have been successfully employed in preparing anisotropically branched metal nanostructures. For ease of discussion, we have classified them into four main strategies (Fig. 1), which will be referred to in this review as (1) seedless growth, (2) seeded growth, (3) templated growth, and (4) chemical etching.

2.1. Seedless growth

Seedless synthesis is a facile one-pot approach that is commonly used for nanocrystal preparation. In the synthesis of branched metal nanostructures, the *in situ* formation of the metal core and the subsequent branching may be affected by the rates of nucleation and growth of

metals, which are critical in determining the final size and morphology. Due to the high symmetry of the *fcc* structure that is adopted by many metals, the formation of branched nanoarchitectures is not an easy matter as factors need to be introduced to break the symmetry. In this subsection, we discuss how twin defects, ions, ligands and polymorphism have been used to facilitate the anisotropic branching of metal nanostructures through the seedless growth route.

2.1.1. Twin-determined branching

A twinned crystal is a symmetrical intergrowth of two or more crystals of the same material. It could form when there is erroneous attachment of adatoms to a growing crystal, resulting in two crystals that are separated by a twin boundary. Metals with low stacking fault energy are highly susceptible to twinning. For *fcc* metals, the formation of multiply-twinned nanocrystals having five-fold symmetry (e.g. decahedron and icosahedron) is thermodynamically favored at very small sizes.¹³ However, as the nanocrystals grow in size, the strain energy caused by twin defects dramatically increases such that the twinned structure can no longer be sustained. Consequently, the twinned structure of the growing nanocrystals evolves into single-crystal structures, such as a truncated octahedron (or Wulff polyhedron) and a cuboctahedron. Moreover, by suitably manipulating the growth conditions, a wide variety of shapes can be obtained at larger sizes.

Xia and co-workers have shown that under appropriate conditions, the five-fold twinned decahedral structure that is initially adopted by their *in situ* generated Rh nanocrystals can evolve into a starfish-like morphology.¹⁴ Their reaction mixture, which consists of $[\{\text{Rh}(\text{CF}_3\text{COO})_2\}_2]$ as the Rh precursor, ethylene glycol as the reductant, and polyvinylpyrrolidone (PVP) as the stabilizer, was heated to 180 °C for a specified time. As shown in Fig. 2A, the Rh nanocrystals that formed in the initial stage of the reaction are multiply-twinned five-fold structures that are mostly in the shape of a decahedron. The cyclic five-fold twinning in a decahedral nanocrystal can be seen in the HRTEM image provided in the inset. The initial formation of Rh nanocrystals having decahedral geometry implies that the reduction reaction occurred under thermodynamic control. With further heating, arms started to grow from the five twin boundary corners of the decahedron along the $\langle 110 \rangle$ direction, eventually transforming the initial nanocrystals into starfish-like nanostructures. Interestingly, this growth behavior is different from what is typically observed for other noble metals, where the starting decahedral nanocrystals evolve into elongated structures (i.e., nanorods and nanowires) with pentagonal cross-sections as a result of axial growth along the five-fold twin junction.^{9, 11, 13} This uniaxial elongation is thought to be promoted by the preferential binding of capping agents on the $\{100\}$ side faces of the growing metal nanocrystals. It is believed that the different growth behavior observed for Rh decahedral nanocrystals is a consequence of the

inability of PVP to effectively passivate the {100} facets of Rh. It is also worth noting that Rh starfish-shaped nanocrystals were not produced when $[\{\text{Rh}(\text{CF}_3\text{COO})_2\}_2]$ was replaced with Na_3RhCl_6 as the Rh precursor, by which irregularly shaped nanostructures were obtained. This is because Na_3RhCl_6 contains Cl^- ions, which, when released during the reaction, can combine with O_2 in air and cause oxidative etching during both the nucleation and growth processes. Because twin defects are highly prone to oxidation and dissolution, oxidative etching makes it difficult to generate nanocrystals with a twinned structure.

Yang et al. have investigated the role of crystal twinning in the formation of nanostructured Pt multipods.¹⁵ They have noted that the final morphology of the Pt nanocrystals is determined by the number of twin planes in the nanocrystals that form at an early stage of crystal growth. In the absence of a twin plane, such as the case of the single-crystal cuboctahedron shown in Fig. 2B(i), the initial nanocrystals transform into nanocubes, which eventually evolve into octapods under conditions that promote growth along the $\langle 111 \rangle$ directions. Meanwhile, the presence of a single twin in the (111) plane leads to planar tripods as illustrated in Fig. 2B(ii). Five-fold twinned decahedral nanocrystals evolve into multipod structures with a rod-like center (Fig. 2B(iii)), whereas other multiply-twinned nanocrystals grow into monopod and multipod structures with a sphere-like core (Fig. 2B(iv)). Changing the reaction conditions (e.g., the capping agent concentration and the reaction temperature) can significantly alter the twinning events and growth kinetics along given directions, which can result in various branched architectures.

2.1.2. Ion-assisted branching

Ion-assisted branching is a method whereby specific ions are purposely added to mediate in branch formation. The ability of silver ions (Ag^+) to induce branching in Au nanocrystals has been demonstrated by Cheng et al. in their seedless synthesis of spiky, urchin-like Au nanostructures (Fig. 3A).¹⁶ Their procedure simply involves mixing HAuCl_4 and AgNO_3 with a moderate amount of ascorbic acid in water. Because $[\text{AuCl}_4]^-$ has a higher reduction potential than Ag^+ , it is preferentially reduced by ascorbic acid to form Au nanocrystals. The essential role of Ag^+ is ascribed to the underpotential deposition of small quantities of Ag^0 onto the surface of the growing Au nanocrystals. The deposited Ag atoms act as active sites that promote the anisotropic growth of Au and this eventually leads to branched architectures. It was noted that decreasing the Ag^+ concentration in solution results in larger but fewer spikes in the final Au nanostructures. However, a popcorn-like structure was obtained when the Ag^+ concentration is too low. In a similar way, Huang and co-workers used cupric ions (Cu^{2+}) to control the anisotropic growth of Pd nanocrystals.¹⁷ The reduction of Cu^{2+} and the subsequent deposition of Cu atoms onto the growing

Pd nanocrystals allow for the directional growth of Pd branches. Meanwhile, Han et al. demonstrated that cuprous ions (Cu^+) can be used to induce crystal twinning in Au nanocrystals.¹⁸ Branching was achieved due to the breaking of the *fcc* symmetry of Au, and this resulted in the formation of Au nanocrosses.

Anions can also play a role in affecting the growth of metal nanostructures. For instance, Xia and co-workers have reported that branched Pt nanostructures can be generated by introducing nitrate anions (NO_3^-) into their polyol system.¹⁹ The shape-directing effect of NO_3^- is shown in Fig. 3B. In the absence of NO_3^- , only Pt nanocrystals with irregular spheroidal morphology were obtained, but the rounded features evolved to more defined facets with increasing amounts of NO_3^- . At sufficiently high concentrations of NO_3^- , the growth of Pt nanocrystals was substantially enhanced at ridges and corners to form multipods. It was suggested that NO_3^- facilitates the anisotropic growth of Pt nanocrystals by changing the reaction pathway for Pt^{4+} reduction. Absorption spectroscopy data revealed that NO_3^- is first reduced to NO_2^- *in situ*, and this is followed by nitroplatinate complex formation due to the ability of NO_2^- to bind strongly to Pt ions. As a consequence, the reduction of Pt ions to Pt^0 is significantly decelerated. This change in reaction kinetics alters the growth rates associated with different crystallographic facets of the Pt nanocrystals, leading to the formation of branched nanostructures.

2.1.3. Ligand-directed branching

The role of capping ligands in controlling the shapes of nanostructured materials has been well established. Ligands possess functional groups that can bind to the nanocrystal surface through an adsorption process called chemisorption. Introduction of a specific type of ligand that can selectively bind to a particular crystallographic facet will lower the energy and slow the growth rate of that facet relative to others, providing a convenient way to facilitate the formation of a branched morphology (Fig. 4A). Chen et al. have recently shown that the presence of the amino acid arginine can direct the formation of Pd tetrapods due to the preferential chemisorption of arginine on Pd {111} facets and its ability to alter the reduction kinetics of the Pd precursor.²⁰ Without arginine, only irregular nanocrystals were obtained. Meanwhile, Zheng and co-workers have shown that introducing methylamine as a surface-controlling ligand generates octapod-shaped Pt nanocrystals with exposed {411} high-index facets.²¹ In their synthesis, both PVP and methylamine were employed as surface capping agents. In the absence of PVP, Pt octapods were still obtained but they are heavily aggregated, implying that the main role of PVP is to passivate and stabilize the Pt nanocrystals. On the other hand, the reaction without methylamine yielded Pt nanocrystals with

mixed morphologies, indicating that the presence of amine is crucial to the formation of the octapod structure. It was also noted that reducing the amount of methylamine significantly lowered the degree of concavity. Their results suggest that the essential role of amine in the formation of the octapod nanocrystals originates from the selective binding of methylamine to the high-index {411} facets of Pt during growth. The effect of varying the nature of surface capping ligands on the final morphology has been demonstrated by Tilley et al. in their shape-controlled synthesis of Pd nanostructures (Fig. 4B).²² When oleylamine (OM) was used solely, isotropic Pd nanocrystals with icosahedral morphology were obtained, suggesting that the growth occurred under thermodynamic conditions. However, introduction of oleic acid (OA) into the surfactant system (1:1 ratio of OA:OM) generated anisotropically branched Pd nanostructures. Note that the carboxylic acid moiety of OA exhibits a weaker binding strength to Pd relative to the amine functionality of OM. Thus, the presence of OA destabilizes the surface of the growing nanocrystals, leading to kinetic growth conditions and anisotropy in the resulting nanocrystals. The OA molecules bind weakly to the faces along the direction of the multipod arms enabling faster growth in these directions.

Lee and co-workers have synthesized branched Au nanocrystals in high yield using a biological buffer molecule, HEPES (i.e., 2-[4-(2-hydroxyethyl)-1-piperazinyl]ethanesulfonic acid), which serves as both the reducing and the shape-directing agent.²³ The resulting Au multipods showed selective tip growth along the <111> directions. The piperazine group in HEPES was identified as the principal moiety that is responsible for the adsorption of the HEPES molecules onto different Au facets, with the binding on the {111} planes being the weakest. A more recent study revealed that at high concentrations, the HEPES molecules self-assemble into long-range ordered structures that help direct the formation of the branched Au nanocrystals.²⁴ Theoretical calculations, supported by experimental results, suggest that the sulfonate group of the HEPES molecules preferably binds to the Au surface, while the free hydroxyl groups facilitate the self-assembly and bilayer formation through hydrogen bonding.

The appropriate choice of ligands is also crucial in the aggregation-based assembly of small metal nanocrystals into highly branched architectures. Ligands with weak to intermediate binding affinity toward the metal ion precursor and toward the *in situ* generated metal nanocrystals are particularly desirable when creating branched structures through the self-aggregation approach. For example, Zou et al. have shown that the use of octadecylamine (ODA) as both the capping agent and the reductant is vital to the formation of Ir nanocrystals having dendritic morphology (Fig 4C).²⁵ Their procedure simply involves heating a mixture of IrCl₃ and ODA at 290 °C under nitrogen flow for 15 min. Investigation of the formation mechanism revealed that during the early stages of the reaction, Ir³⁺ is gradually reduced to Ir and this initially yields small Ir nanocrystals. With further

heating, the initially formed Ir nanocrystals gradually evolve into nanodendrites through self-aggregation. The gradual reduction of Ir³⁺ to Ir is regulated by ODA, which has a weak binding affinity to Ir³⁺. Moreover, the ineffective stabilization by ODA promotes the coalescence and self-aggregation of the weakly passivated Ir nanocrystals. When trioctylphosphine (TOP), a more effective stabilizer, was used in combination with ODA, only quasi-spherical Ir nanocrystals were obtained. This is because TOP, with its strong coordinating ability, can form a stable complex with Ir³⁺ and this delays the nucleation process as the reduction of Ir³⁺ to Ir by ODA is hindered. Also, TOP is able to effectively cap the surface of the initially formed Ir nanocrystals and so the growth of well-passivated spherical nanocrystals through atomic addition is favored over self-aggregation. The ligand-controlled self-aggregation approach to branched metal nanostructures has also been employed in the synthesis of Pd nanodendrites.²⁶

2.1.4. Polymorphism-induced branching

It is well known that the polymorphism inherent in some semiconductors can be utilized in the construction of branched semiconductor nanostructures, such as in the case of cadmium chalcogenide semiconductors which exhibit two polymorphic forms (i.e., zinc-blende and wurtzite). This approach has been recently adopted by Tilley et al. for the synthesis of branched metal nanostructures, where the *fcc-hcp* polymorphism inherent in Ni metal was exploited to generate Ni nanostructures that consist of an *fcc* Ni core and arms that grow with alternating *fcc* and *hcp* phases.²⁷ Their procedure involves the thermal decomposition and reduction of Ni(acac)₂ (where acac = acetylacetonate) in mesitylene under hydrogen atmosphere and in the presence of hexadecylamine (HDA) and trioctylphosphine (TOP) as capping ligands. It was found that aside from the effect of polymorphism, the TOP ligand also plays an important role in promoting the formation of branched structures. Time-dependent experiments revealed that at earlier reaction times, truncated octahedral *fcc* Ni nanocrystals are initially formed. These *fcc* nanocrystals are bound by six {100} and eight {111} facets. Because of the preferential binding of TOP molecules to the {100} facets, only the {111} facets of the truncated cuboctahedron core experienced further growth that leads to branch formation. Due to the presence of stacking faults along the [111] direction, the {111} *fcc* facets grow to become {001} *hcp* facets. The alternating *fcc* and *hcp* segments in the nanocrystal arms are believed to be a result of the interplay between kinetic growth conditions, phase stability and surface energies.

2.2. Seeded growth

In seeded growth, pre-synthesized seeds are utilized to serve as nucleation points for the

anisotropic growth of branched metal nanostructures. In terms of ease of manipulation, the seeded growth approach may not be the most convenient method as it is not a one-step process but it certainly has its own merits. For instance, it is often a challenge to tune the crystallite size over a wide range when employing one-step synthetic protocols, as increasing the initial precursor concentrations may lead to more nucleation events that may reduce the driving force for nanocrystal growth. In seeded growth, the use of pre-synthesized seeds distinctly separates the nucleation event from the growth stage, allowing precise control over the nanocrystal size.²⁸ Another advantage of the seeded growth strategy is that the size, shape and composition of the seeds can be used to control the morphology of the target nanostructures. This is illustrated in the examples discussed below.

Xia and co-workers have reported that the use of Au nanocrystal seeds with octahedral morphology can lead to the formation of Au nanohexapods (Fig. 5A).²⁹ Their synthetic protocol involves the reduction of HAuCl_4 by dimethylformamide (DMF) in water in the presence of pre-synthesized Au nano-octahedra. The resultant Au atoms preferentially nucleated and grew from the six vertices of the octahedral-shaped Au seeds, leading to the formation of Au nanohexapods that consist of an octahedral core and six arms that protrude from all the vertices. This is in accordance with the crystal growth theory, which predicts that growth rates would be greatest at the highest energy features of the seeds (i.e., the six vertices of each octahedron). The length of the arms can be readily controlled by varying certain experimental parameters, such as the amount of HAuCl_4 and the reaction temperature. Meanwhile, Skrabalak et al. have shown that co-reduction of HAuCl_4 and H_2PdCl_4 by ascorbic acid in the presence of octahedral-shaped Au seeds of suitable size produces branched Au–Pd bimetallic nanocrystals at sufficiently high pH values.^{30–32} Because of the higher reduction potential of HAuCl_4 , Au was found to deposit first on the pre-existing Au seeds. This is followed by branched overgrowth and then by deposition of Pd on the surfaces particularly on the branch tips, leading to heterostructured nanocrystals that possess an Au-rich interior with eight uniform Pd-tipped branches. Surprisingly, the branches seemed to have preferentially grown from the eight $\{111\}$ facets rather than the six vertices of the octahedral seeds. However, further investigations revealed that the octahedral Au seeds undergo restructuring during growth to form cubic-like structures prior to branch formation (Fig. 5B).³² Thus, the eight arms actually grew from the eight vertices of the cubic intermediates. The effect of the seed composition on the final nanostructure morphology was also studied by using Pd in place of Au seeds.^{32, 33} It was found that while the Au seeds undergo structural changes during growth, the Pd seeds are structurally stable. Branch growth occurred from the six high-energy vertices of the octahedral Pd seeds. Interestingly, four branches emerged from each of the six vertices, producing a total of 24

branches per nanocrystal. By contrast, three branches per vertex were observed when tetrahedral Pd seeds were used (i.e., total of 12 branches per nanocrystal as a tetrahedron has four vertices). It was suggested that the number and acuteness of the vertices coupled with the crystallographic orientation of the vertices relative to available growth directions account for the different number of branches emerging per vertex.³³

Through overgrowth of Au onto pre-made Pt nanocrystal seeds, Sun and co-workers were able to prepare branched Pt–Au_{*n*} nanoscale heterostructures, where the number (*n*) of Au branches in each particle can be controlled from 1 to 4 by tuning the size of the Pt seeds.³⁴ On the basis of Monte Carlo simulation, they proposed that the morphological growth is regulated by a thermodynamic equilibrium of the Au coherence energy, the overall particle surface energy, and the heterogeneous Pt–Au interfacial energy in the system. Guided by this important insight and the fact that selective growth of a heterogeneous nanocrystal phase onto certain regions of nanocrystal seeds depends on the surface potential and lattice matching, Cheng and co-workers have created branched Pt–Au_{*n*} nanoarchitectures with predetermined composition and morphology.³⁵ In this structure-guided approach, highly monodisperse Pt nanocubes were used as seeds. Because of the excellent lattice coherence between Pt and Au crystals in the *fcc* phase, the epitaxial growth of Au preferentially occurred at the vertices of the cubic Pt seeds as seen in Fig. 5C. The number of Au branches was found to increase with increasing seed size as a result of reduced steric hindrance.

2.3. Templated growth

Template-assisted growth is another approach that can be employed to facilitate branching of nanostructured materials. The template provides the necessary structural framework, within or around which the nanostructure forms and grows into a shape that is complementary to that of the template. Xia and co-workers have successfully demonstrated the use of an array of magnetic Fe nanoparticles for the templated synthesis of branched Au nanostructures.³⁶ In their work, the template does not only serve as a scaffold, but also participates in the chemical reaction and spontaneously falls apart at a certain point to release the desired product. A schematic depiction of the process and the corresponding TEM images are displayed in Fig. 6A. The template is a three-dimensional (3D) porous lattice consisting of uniform quasi-spherical Fe nanoparticles that are self-assembled on a magnetic stir bar. Upon addition of AuCl, a galvanic replacement reaction between Fe and Au⁺ takes place. The Au atoms that are produced in this reaction begin to nucleate and eventually grow into multipods within the void spaces in between the Fe nanoparticles. The consumption of Fe and the volume expansion associated with the replacement of Fe with Au

gradually weakened the magnetic attraction between the Fe nanoparticles. As a result, the lattice of Fe nanoparticles eventually self-destructs and automatically releases the Au multipods. Any remaining Fe nanoparticles were readily removed by washing the samples with acids.

Deep eutectic solvent (DES) is another template that has been utilized in the synthesis of branched metal nanostructures in solution. It is a type of ionic solvent that can form extended hydrogen-bond systems in the liquid state and this unique quality has allowed their use in the construction of well-defined and ordered nanoscale structures. As an example, Sun and co-workers have reported a facile method to prepare branched Au nanostructures by reducing HAuCl_4 with ascorbic acid in DES at 30 °C.³⁷ It is worth noting that their procedure does not require the use of any adsorbates, surfactants or seeds, but simply utilizes DES, which serves as the solvent, the stabilizer and the liquid template. It is known that the water content in DES can alter the structural features of the template, and this can be used to control the morphology of the Au nanocrystals. It was observed that with increasing water content, the morphology of the Au nanostructures turned from snowflake-like (no water) to star-shaped (5000 ppm water) to thorny (>10000 ppm water). Meanwhile, a recent report by Liu et al. has shown that graphene oxide (GO) nanosheets can be used as a scaffold for the formation of highly branched Au nanoarchitectures enriched with a uniform facet.³⁸ GO is a monolayer of two-dimensional (2D) honeycomb lattice of carbon atoms whose basal planes and edges are laden with numerous oxygen-containing functionalities (i.e., carboxyl, hydroxyl and epoxy groups). During the ethanol-assisted reduction of the Au precursor, the oxygen-containing moieties serve as implantation sites for the *in situ* nucleation and the subsequent diffusion-limited growth of well-defined branched Au nanostructures. In the absence of GO nanosheets, only ill-defined irregular Au nanocrystals were obtained.

Baigl and co-workers have reported the use of branched DNA–protein assemblies as a template for the formation of branched Ag nanostructures (Fig. 6B).³⁹ Here, the branched biological template is composed of one to four biotinylated DNA molecules that are conjugated to a single streptavidin protein core. Note that streptavidin is a tetrameric biotin-binding protein that can bind up to four biotinylated molecules. Templated metallization was carried out through successive addition of AgNO_3 and NaBH_4 (i.e., the reducing agent), resulting in Ag nanostructures with one to four branches of well-defined lengths. With this method, it is possible to tune two structural parameters: (i) the degree of branching by varying the concentration of streptavidin and (ii) the branch length by using biotinylated DNA molecules of different lengths. Branched Cu nanostructures have also been prepared using a similar DNA-templated approach.⁴⁰

2.3. Chemical etching

The chemical etching strategy creates branched nanostructures through selective dissolution of certain crystallographic facets using etchants. Tuning of the etchant strength enables the preparation of different nanostructure shapes in high yield and purity. For example, Yang and co-workers have formulated a highly selective etchant solution to achieve a series of morphological transformations in Ag nanocrystals (Fig. 7A).⁴¹ Their etchant formulation, 9:1 $\text{NH}_4\text{OH}/\text{H}_2\text{O}_2$, exhibits a high degree of selectivity for etching of $\{100\}$ crystal faces over $\{111\}$ faces of octahedral-shaped Ag nanocrystals. Increasing the etchant concentration increases the preferential etching in the $[100]$ direction, eventually transforming the initial nano-octahedra into nano-octapod structures.

In a report by Xiong et al., it was demonstrated how oxidative etching in the presence of varying amounts of HCl can lead to the formation of branched Pt nanocrystals with different number of branches (Fig. 7B).⁴² The Pt nanocrystals were prepared by heating a mixture that consists of H_2PtCl_6 , PVP (i.e., the stabilizer), KBr, ethylene glycol (i.e., the reducing agent) and water in air. By adding different amounts of HCl to the reaction system, they were able to tune the crystallinity of the initial Pt nanocrystals and the modes of atomic addition. Basically, the acidity of HCl can greatly enhance the etching strength of O_2 and Cl^- . Without HCl, it was found that the Pt nanocrystals that initially formed are singly-twinned triangular nanoplates, which eventually grew into tripod-like structures. By contrast, the presence of HCl led to the initial formation of single-crystal cuboctahedral Pt nanocrystals, which evolved into multiply-branched structures. The number of branches were observed to increase from 4 (tetrapod) to 6 (hexapod) to 8 (octapod) with increasing amount of HCl. Meanwhile, Tilley and co-workers observed an unusual etching process in the formation of branched Pt nanostructures that were synthesized under hydrogen atmosphere.⁴³ Pt nano-octapods were generated when a high concentration of the Pt precursor, $\text{Pt}(\text{acac})_2$, was used. Synchrotron-based XRD and TEM data revealed that the octapods evolved from cuboctahedral nanocrystals through an etching process that dissolved the $\{100\}$ faces with simultaneous overgrowth along the $\{111\}$ directions. Because the reaction was carried out in the absence of O_2 and halide etchants and since etching was only observed when using sufficiently high concentrations of $\text{Pt}(\text{acac})_2$, it was believed that the etchant species originated from acetylacetonate, possibly its enol form which has been known to etch metal surfaces *via* a chelation process.

3. Properties and Applications

The morphological features that are unique to branched metal nanostructures endow them with novel properties that can be utilized in a wide array of applications. In this section, we highlight their

potential utility in the areas of plasmonics, biomedicine and catalysis.

3.1 Plasmonics

Metal nanostructures are excellent light scatterers and absorbers due to their enhanced surface plasmon resonance (SPR), an optical phenomenon that arises from the interaction of electromagnetic waves with the conduction electrons in metals. The SPR-based optical properties of metal nanostructures can be easily tuned by altering their morphology. As an example, the etching-induced morphological transformation (i.e., from octahedron to octapod) observed in Ag nanocrystals have resulted in intraparticle coupling effects that have significantly altered the plasmonic features of the original structure.⁴¹ While the starting Ag nano-octahedra displayed strong plasmonic peaks in the visible range, the final Ag nano-octapods showed intense plasmonic bands in the red and the near-infrared (NIR) region. Furthermore, the nano-octapods have been found to exhibit single-particle SERS signals that are 30 times stronger than those of the original nano-octahedra, indicating their potential utility as Raman sensors.

Hupp et al. have shown that the SPR peaks of branched Au nanostructures are red-shifted by 130–180 nm from those of spherical Au nanocrystals.⁴⁴ This observation is consistent with the results of their discrete dipole approximation (DDA) calculations, which also revealed that the largest field enhancements occur at the tips of the branched structures. In a study by Walker and co-workers, the Raman enhancement factors of star-shaped Au nanostructures have been evaluated and compared with those of Au nanospheres and nanorods of comparable sizes.⁴⁵ Crystal violet (CV) and 2-mercaptopyridine (2-MPy) were used as probe molecules in the study. It was found that the nanostars produced more enhanced Raman signals than the nanospheres for both probe molecules. Although the Raman enhancement by nanostars and nanorods was similar for 2-MPy, it was significantly higher for nanostars for CV, particularly at low concentrations of the probe molecule.

The plasmonic properties of branched Au nanostructures with unique cross-like morphology have been investigated by Han et al.^{18, 46} A representative TEM image and the reconstructed 3D tomography of a single Au nanocross are shown in Figs. 8A and 8B, respectively. TEM data revealed that these Au nanocrosses possess two longer branches that extend along the $\langle 110 \rangle$ direction and two shorter branches that extend along the $\langle 001 \rangle$ direction. Meanwhile, their absorption spectrum (Fig. 8C) showed well-defined localized surface plasmon features – a less intense peak centered at around 550 nm and an intense broad absorption covering the NIR region (i.e., from 800 to 1200 nm). The peak around 550 nm is attributed to the transverse dipolar resonance of the branches, whereas the broad absorption in the NIR range arises from

the dipolar resonance of the branches that is similar to the longitudinal mode observed in Au nanorods. In order to quantify the precise optical response of the Au nanocrosses, monochromated electron energy-loss spectroscopy (EELS) was used to probe surface plasmon kinetics and damping in a single nanostructure.⁴⁶ A single nanocross that carries three main plasmon modes was studied as an example. EELS plasmon maps (Fig. 8D) were extracted, colour-coded and assigned the Q (quality factor) and T_2 (dephasing time) values that result from analysis of the EELS spectra shown in Figs. 8E and 8F. The variances for Q and T_2 were calculated from the sample standard deviation propagating from the Lorentzian fitting to the four spectra from locations I–IV shown in Fig. 8D. The quality factor, Q , is a measure of the enhancement of the oscillation amplitude of a driven oscillating system with respect to the driving amplitude (i.e., the local-field enhancement in the case of particle plasmons).⁴⁷ This value is a figure of merit for all nonlinear applications of particle plasmons such as SERS. Many optical applications also require that the dephasing of the particle plasmon be as slow as possible, which means that the dephasing time, T_2 , should be as long as possible. The relatively higher Q and T_2 values observed for Au nanocrosses compared to those reported for Au nanospheres is a strong implication that these branched Au nanostructures are better suited for optical applications, especially where large local-field enhancements are necessary.

3.2 Biological applications

Biological applications, which include photothermal therapy and biomedical imaging and detection, make use of light in the NIR spectral window to achieve deep penetration into soft tissues. Han et al. have shown that Au nanocrosses, with their strong absorption in the NIR range, can be utilized as efficient absorbers for photothermal destruction of living cells upon NIR irradiation.¹⁸ In order to prove the effectiveness of Au nanocrosses for photothermal therapy, experiments using human lung cancer cells (A549) were conducted. Fig. 9A shows that in the presence of Au nanocrosses, the cancer cells died very rapidly within 30 s of 900-nm laser irradiation at $\sim 4.2 \text{ W/cm}^2$. This was not observed in control experiments that were carried out in the absence of Au nanocrosses, where the cancer cells remained alive even after 10 min of irradiation. In addition to photothermal therapy, Au nanocrosses can also be used for two-photon luminescence imaging. To further understand how the cancer cells were destroyed during photothermal therapy, two-photon luminescence imaging was used to study the distribution of Au nanocrosses associated with cells (Fig. 9B). Initially, the Au nanocrosses were found mainly on the membranes of the cells. However, the cells shrunk immediately in both size and shape within 30 s of laser exposure, and the collapsed cell membranes brought the Au

nanocrosses together to form agglomerates. These results clearly indicate the high photothermal efficacy of Au nanocrosses. Theoretical calculations using DDA was conducted to simulate the synergistic coupling among 1, 2, 3, or 4 branches of a single nanocross. It was found that the entire nanocross can be excited to participate in light absorption even if only one of the branches is exposed to incident light. This property makes them useful as octopus antennas that can efficiently capture incident IR light and convert it into heat for ultrafast photothermal destruction of cancer cells.

Xia et al. have demonstrated the utility of Au nanohehexapods in both photothermal therapy and contrast-enhanced diagnosis.⁴⁸ Prior to use, the nanostructures were coated with polyethylene glycol (PEG) to achieve biocompatibility. The PEGylated Au nanohehexapods exhibited high cellular uptake and low cytotoxicity *in vitro*. Moreover, they showed significant blood circulation and tumor accumulation after intravenous injection. When compared with PEGylated Au nanocages and Au nanorods, the PEGylated Au nanohehexapods exhibited the highest photothermal conversion efficiency *in vivo*. The photothermal treatment effect on tumor metabolic activity was assessed using ¹⁸F-fluorodeoxyglucose positron emission tomography combined with computed tomography (¹⁸F-FDG PET/CT). Fig. 9C shows that the ¹⁸F-FDG uptake was significantly reduced in the irradiated tumors in contrast to the contralateral non-irradiated tumors. There was approximately 90% reduction of tumor metabolism in mice treated with Au nanohehexapods, indicating almost complete destruction of tumor glycolic activity following photothermal treatment. From these results, it can be concluded that branched Au nanostructures are promising materials for cancer theranostics as both photothermal transducer and diagnostic agent.

3.3 Catalysis

Branched metal nanostructures are also of considerable interest in catalysis, owing to their large specific surface area, tips with small radii of curvatures and high densities of edges, corners, and stepped atoms. The effect of varying the number of branches on the catalytic activity has been investigated by Xiong et al. using a series of nanostructured Pt multipods having 3, 4, 6 and 8 branches.⁴² Fig. 10A shows that the catalytic activity for formic acid oxidation increases with increasing number of branches and this can be attributed to the higher density of stepped surface atoms and the larger surface area of the more branched structures. When compared to the commercial Pt/C (i.e., carbon-supported Pt nanoparticles) catalyst, only the 6- and 8-armed Pt multipods exhibited superior electrocatalytic performance. Meanwhile, Xia et al. have reported that their Pd–Pt bimetallic nanodendrites exhibit better catalytic activity

as a fuel cell electrocatalyst than the commercial Pt/C catalyst and the fuel-cell grade Pt-black catalyst.⁴⁹ The nanodendrites, which were prepared through seeded growth, consist of a dense array of multiple Pt branches that surround a faceted Pd core. Their dendritic morphology renders them with a reasonably high surface area despite their relatively large overall particle size. Furthermore, the multiply-branched architecture exposes a large number of facets that are particularly active toward the oxygen reduction reaction (ORR), which is the rate-determining step in a proton-exchange membrane (PEM) fuel cell. At room temperature, the Pd–Pt nanodendrites are 2.5 times more active on the basis of equivalent Pt mass for the ORR than the Pt/C catalyst and 5 times more active than the Pt-black catalyst. In addition to the mass activity, the Pd–Pt nanodendrites also exhibited a specific activity that is superior to that of Pt/C and Pt-black, as shown in Fig. 10B. This demonstrates the accelerated ORR kinetics on the surfaces of the Pd–Pt nanodendrites. In a separate study, Wang and co-workers have successfully prepared Pd–Pt bimetallic nanodendrites supported on graphene nanosheets by growing Pt branches directly on the graphene-supported Pd nanocrystal seeds.⁵⁰ This nanostructured metal–graphene hybrid exhibits mass activity for the methanol oxidation reaction that is about 3.0 and 9.5 times greater than that of the commercial Pt/C and Pt-black catalysts, respectively. With these results, it is clear that branched metal nanostructures hold enormous potential as electrocatalysts for fuel cell applications.

The catalytic behavior of Pd multipods has been evaluated for the reduction of hexavalent Cr (Cr^{6+}) to trivalent Cr (Cr^{3+}) by Chen et al.²⁰ As Cr^{6+} is known to be carcinogenic, it is highly desirable to develop an efficient catalyst system for its conversion to Cr^{3+} , which is nontoxic. The reduction of $\text{K}_2\text{Cr}_2\text{O}_7$, a Cr^{6+} compound, by formic acid was chosen as a model reaction to study. As one can see in Fig. 10C, the characteristic absorption peak of Cr^{6+} vanishes within 5 min, accompanying a color change from yellow to colorless, in the presence of Pd nanotetrapods. By contrast, it took a longer time (ca. 20 min) for the absorption band to disappear when commercial Pd-black was used as the catalyst. Another important catalytic reaction is the reduction of 4-nitrophenol by NaBH_4 to produce 4-aminophenol, a chemical reagent that is widely utilized in many industrial applications. Liu et al. have shown that branched Au nanostructures enriched with a uniform facet display far better activity for catalytic reduction of 4-nitrophenol than spherical Au nanostructures exposed with mixed facets.³⁸ These results further demonstrate the excellent catalytic behavior of metal nanostructures having branched morphologies.

4. Summary and outlook

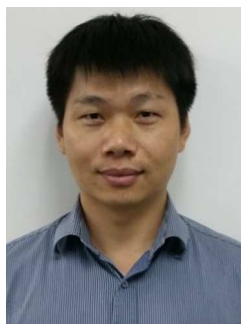
Recent years have witnessed a flourishing interest on the shape-controlled synthesis of metal nanostructures. This is evidenced by the rapidly growing number of publications on metal nanostructures of various shapes or morphologies. While many of the previously published review papers have placed focus on metal nanocrystals with simpler and more common shapes, such as spheres, rods, and cubes, this tutorial review shines the spotlight on anisotropically branched metal nanostructures with geometries that can be described as similar to multipods, stars, crosses, urchins and dendrites. The synthesis of this class of metal nanostructures has drawn considerable attention owing to the enhanced properties that result from their branched architectural features. Discussed in this review are four solution-based strategies that are typically employed in the synthesis of branched metal nanostructures: (1) seedless growth, (2) seeded growth, (3) templated growth, and (4) chemical etching. *Seedless growth* is a convenient one-pot synthetic strategy that does not make use of pre-synthesized seeds to facilitate branching. Instead, it relies on foreign ions and capping ligands that are deliberately added to mediate in branch formation. In some cases, crystal twinning and polymorphism can also be exploited to induce branching. *Seeded growth*, on the other hand, is a two-step process that begins with the synthesis of small metal nanocrystals, which are then utilized as seeds whose surfaces can promote the formation of branched architectures. While it is not the most facile approach, the seeded growth strategy enables precise control over size as a consequence of the separate nucleation and growth stages. Furthermore, the size, shape and composition of the seeds can be used to control the number of branches in the final nanostructures. Bimetallic nanostructures (e.g. Pt core with Au branches) are also easily achieved through this synthetic approach. As the name implies, the *templated growth* strategy involves the use of a template whose structural features can facilitate the nucleation and growth of branched nanoarchitectures. A wide variety of materials can be employed as templates, which include deep eutectic solvents, nanoparticle arrays, and DNA–protein assemblies. Meanwhile, the *chemical etching* route achieves branching *via* selective dissolution of certain crystallographic facets using chemical etchants. In this approach, the degree of branching can be conveniently controlled by adjusting the concentration of the etchant.

The successful synthesis of anisotropically branched metal nanostructures has enabled scientists to explore their properties as well as their potential applications, particularly in the areas of plasmonics, biomedicine and catalysis. However, most of the reports on branched metal nanostructures that have been published to date are quite limited to a few noble metals like Au, Pt and Pd. For instance, both Au and Ag are regarded as prime candidates for SERS detection and

cancer theranostics due to their remarkable plasmonic and photothermal properties but reports on branched Ag nanostructures are much less common than those of their Au counterparts. Ag is less expensive and has a stronger plasmonic response than Au but it is often less favored due to its inferior stability, which limits its usefulness in certain applications. It is anticipated that the synthesis of suitably functionalized branched Ag nanostructures that are stable under many different conditions (e.g. in biologically relevant media) would make Ag a better alternative to Au in plasmonic and biomedical applications. Alloyed branched nanostructures based on Au and Ag also merit further studies as plasmonic response and stability can be improved through appropriate combination of different metals. In the field of catalysis, the most extensively investigated branched metal nanostructures are those of Pt and Pd but there are a number of other catalytic metals whose branched structures are worthy of further investigation. For instance, Rh and Ir have been found useful in a wide range of catalytic reactions but their use in practical applications is limited by the very high cost of these metals, which are two of the rarest elements in the Earth's crust. A branched architecture is expected to dramatically enhance the catalytic efficiency of Rh and Ir nanostructures, and this would help in substantially reducing the loading amount of these precious metals in catalytic processes. Meanwhile, Fe, Co and Ni are well known not only for their catalytic properties but also for their magnetic properties. The synthesis of branched nanostructures of these metals and their alloys may lead to important discoveries that have never been previously reported.

We anticipate that, in the coming years, more versatile and facile methods for the preparation of anisotropically branched metal nanostructures will be developed, so that such branched nanocrystals can be obtained in a controllable and reproducible manner, and more sophisticated architectures can be designed. The ability to synthesize metal nanostructures with more complex branching may lead to the emergence of new properties that will cater for a wider range of applications. However, better understanding of the growth mechanisms and structure–property correlations is still necessary to accelerate the advancement of technologies based on branched metal nanostructures. Furthermore, challenges associated with stability and scaling-up capability still need to be overcome before this class of metal nanostructures can be commercialized.

Authors



Enyi Ye obtained his PhD in Chemistry from the National University of Singapore. He presently works as a research scientist at the Institute of Materials Research and Engineering under the Agency for Science, Technology and Research (A*STAR) in Singapore. His research is centered on the synthesis, properties and applications of nanostructured materials, such as semiconductor, metallic, metal oxide and luminescent lanthanide-based nanocrystals.



Michelle D. Regulacio received her PhD in Chemistry from Georgetown University. She was a postdoctoral research associate in the Department of Chemistry at Princeton University before joining the Institute of Materials Research and Engineering as a research scientist. Her research focuses on the colloidal chemical synthesis and potential technological applications of inorganic nanoscale materials, which include alloyed semiconductor nanocrystals and hybrid nanostructures.



Shuang-Yuan Zhang received his PhD in Integrative Sciences and Engineering from the National University of Singapore. He currently works as a research scientist at the Institute of Materials Research and Engineering. His research is centered on the solution-based synthesis and self-assembly of functional nanostructures and their corresponding thermal, optical, magnetic, and catalytic applications.



Xian Jun Loh is the Head of Research Planning at the Institute of Materials Research and Engineering and assistant professor at the National University of Singapore (NUS). He obtained his PhD in 2009 from NUS. In 2011, he was elected into the Fellowship at Fitzwilliam College, Cambridge. His main interests are in the design of supramolecular and stimuli-responsive

polymers and hydrogels for biomedical applications.



Ming-Yong Han obtained his PhD in Chemistry from Jilin University. He was with IBM and Indiana University before his current appointment as senior scientist with the Institute of Materials Research & Engineering. His research addresses problems at the interfaces of nanoscience, nanotechnology, biotechnology and optoelectronics.

References

1. S. Cheong, J. D. Watt and R. D. Tilley, *Nanoscale*, 2010, 2, 2045-2053.
2. H. Zhang, M. Jin, Y. Xiong, B. Lim and Y. Xia, *Accounts of Chemical Research*, 2012, 46, 1783-1794.
3. P. K. Jain, X. Huang, I. H. El-Sayed and M. A. El-Sayed, *Accounts of Chemical Research*, 2008, 41, 1578-1586.
4. K. Xia, L. Zhang, Y. Huang and Z. Lu, *Journal of Nanoscience and Nanotechnology*, 2015, 15, 63-73.
5. M. Hu, J. Chen, Z.-Y. Li, L. Au, G. V. Hartland, X. Li, M. Marquez and Y. Xia, *Chemical Society Reviews*, 2006, 35, 1084-1094.
6. S. Pal, Y. K. Tak and J. M. Song, *Applied and Environmental Microbiology*, 2007, 73, 1712-1720.
7. M. Faraday, *Philosophical Transactions of the Royal Society of London*, 1857, 147, 145-181.
8. G. Wulff, *Zeitschrift für Kristallographie-Crystalline Materials*, 1901, 34, 449-530.
9. Y. Xia, Y. Xiong, B. Lim and S. E. Skrabalak, *Angewandte Chemie International Edition*, 2009, 48, 60-103.
10. H. You, S. Yang, B. Ding and H. Yang, *Chemical Society Reviews*, 2013, 42, 2880-2904.
11. A. R. Tao, S. Habas and P. Yang, *Small*, 2008, 4, 310-325.
12. B. Lim and Y. Xia, *Angewandte Chemie International Edition*, 2011, 50, 76-85.
13. J. L. Elechiguerra, J. Reyes-Gasga and M. J. Yacaman, *Journal of*

- Materials Chemistry*, 2006, 16, 3906-3919.
14. H. Zhang, X. Xia, W. Li, J. Zeng, Y. Dai, D. Yang and Y. Xia, *Angewandte Chemie International Edition*, 2010, 49, 5296-5300.
 15. S. Maksimuk, X. Teng and H. Yang, *Journal of Physical Chemistry C*, 2007, 111, 14312-14319.
 16. L.-C. Cheng, J.-H. Huang, H. M. Chen, T.-C. Lai, K.-Y. Yang, R.-S. Liu, M. Hsiao, C.-H. Chen, L.-J. Her and D. P. Tsai, *Journal of Materials Chemistry*, 2012, 22, 2244-2253.
 17. Y.-T. Chu, K. Chanda, P.-H. Lin and M. H. Huang, *Langmuir*, 2012, 28, 11258-11264.
 18. E. Ye, K. Y. Win, H. R. Tan, M. Lin, C. P. Teng, A. Mlayah and M.-Y. Han, *Journal of the American Chemical Society*, 2011, 133, 8506-8509.
 19. T. Herricks, J. Chen and Y. Xia, *Nano Letters*, 2004, 4, 2367-2371.
 20. G.-T. Fu, X. Jiang, R. Wu, S.-H. Wei, D.-M. Sun, Y.-W. Tang, T.-H. Lu and Y. Chen, *ACS Applied Materials & Interfaces*, 2014, 6, 22790-22795.
 21. X. Huang, Z. Zhao, J. Fan, Y. Tan and N. Zheng, *Journal of the American Chemical Society*, 2011, 133, 4718-4721.
 22. J. Watt, N. Young, S. Haigh, A. Kirkland and R. D. Tilley, *Advanced Materials*, 2009, 21, 2288-2293.
 23. J. Xie, J. Y. Lee and D. I. Wang, *Chemistry of Materials*, 2007, 19, 2823-2830.
 24. H. Liu, Y. Xu, Y. Qin, W. Sanderson, D. Crowley, C. H. Turner and Y. Bao, *The Journal of Physical Chemistry C*, 2013, 117, 17143-17150.
 25. C. Wang, G. Xiao, Y. Sui, X. Yang, G. Liu, M. Jia, W. Han, B. Liu and B. Zou, *Nanoscale*, 2014, 6, 15059-15065.
 26. N. Ortiz and S. E. Skrabalak, *Angewandte Chemie International Edition*, 2012, 51, 11757-11761.
 27. A. P. LaGrow, S. Cheong, J. Watt, B. Ingham, M. F. Toney, D. A. Jefferson and R. D. Tilley, *Advanced Materials*, 2013, 25, 1552-1556.
 28. C. Gao, J. Goebel and Y. Yin, *Journal of Materials Chemistry C*, 2013, 1, 3898-3909.
 29. D. Y. Kim, T. Yu, E. C. Cho, Y. Ma, O. O. Park and Y. Xia, *Angewandte Chemie International Edition*, 2011, 123, 6452-6455.
 30. C. J. DeSantis, A. A. Peverly, D. G. Peters and S. E. Skrabalak, *Nano Letters*, 2011, 11, 2164-2168.
 31. C. J. DeSantis, A. C. Sue, M. M. Bower and S. E. Skrabalak, *ACS Nano*, 2012, 6, 2617-2628.
 32. R. G. Weiner, C. J. DeSantis, M. B. Cardoso and S. E. Skrabalak, *ACS Nano*, 2014, 8, 8625-8635.
 33. C. J. DeSantis and S. E. Skrabalak, *Journal of the American Chemical Society*, 2012, 135, 10-13.
 34. C. Wang, W. Tian, Y. Ding, Y.-q. Ma, Z. L. Wang, N. M. Markovic, V. R. Stamenkovic, H. Daimon and S. Sun, *Journal of the American Chemical Society*, 2010, 132, 6524-6529.
 35. K. Cheng, S.-R. Kothapalli, H. Liu, A. L. Koh, J. V. Jokerst, H. Jiang, M. Yang, J. Li, J. Levi and J. C. Wu, *Journal of the American Chemical Society*, 2014, 136, 3560-3571.
 36. Z. Li, W. Li, P. H. Camargo and Y. Xia, *Angewandte Chemie International Edition*, 2008, 47, 9653-9656.
 37. H. G. Liao, Y. X. Jiang, Z. Y. Zhou, S. P. Chen and S. G. Sun, *Angewandte Chemie International Edition*, 2008, 120, 9240-9243.
 38. M. Zhu, B. Lei, F. Ren, P. Chen, Y. Shen, B. Guan, Y. Du, T. Li and M. Liu, *Scientific Reports*, 2014, 4.
 39. S. Rudiuk, A. Venancio-Marques, G. Hallais and D. Baigl, *Soft Matter*, 2013, 9, 9146-9152.
 40. H. A. Becerril, R. M. Stoltenberg, D. R. Wheeler, R. C. Davis, J. N. Harb and A. T. Woolley, *Journal of the American Chemical Society*, 2005,

- 127, 2828-2829.
41. M. J. Mulvihill, X. Y. Ling, J. Henzie and P. Yang, *Journal of the American Chemical Society*, 2010, 132, 268-274.
 42. L. Ma, C. Wang, M. Gong, L. Liao, R. Long, J. Wang, D. Wu, W. Zhong, M. J. Kim and Y. Chen, *ACS Nano*, 2012, 6, 9797-9806.
 43. S. Cheong, J. Watt, B. Ingham, M. F. Toney and R. D. Tilley, *Journal of the American Chemical Society*, 2009, 131, 14590-14595.
 44. E. Hao, R. C. Bailey, G. C. Schatz, J. T. Hupp and S. Li, *Nano Letters*, 2004, 4, 327-330.
 45. E. N. Esenturk and A. R. Hight Walker, *Journal of Raman Spectroscopy*, 2009, 40, 86-91.
 46. M. Bosman, E. Ye, S. F. Tan, C. A. Nijhuis, J. K. Yang, R. Marty, A. Mlayah, A. Arbouet, C. Girard and M.-Y. Han, *Scientific Reports*, 2013, 3.
 47. C. Sonnichsen, T. Franzl, T. Wilk, G. von Plessen, J. Feldmann, O. Wilson and P. Mulvaney, *Physical Review Letters*, 2002, 88, 077402-077402.
 48. Y. Wang, K. C. Black, H. Luehmann, W. Li, Y. Zhang, X. Cai, D. Wan, S.-Y. Liu, M. Li and P. Kim, *ACS Nano*, 2013, 7, 2068-2077.
 49. B. Lim, M. Jiang, P. H. Camargo, E. C. Cho, J. Tao, X. Lu, Y. Zhu and Y. Xia, *Science*, 2009, 324, 1302-1305.
 50. S. Guo, S. Dong and E. Wang, *ACS Nano*, 2009, 4, 547-555.

Anisotropically Branched Metal Nanostructures

Enyi Ye,⁺ Michelle D. Regulacio,⁺ Shuang-Yuan Zhang, Xian Jun Loh, Ming-Yong Han*

FIGURES

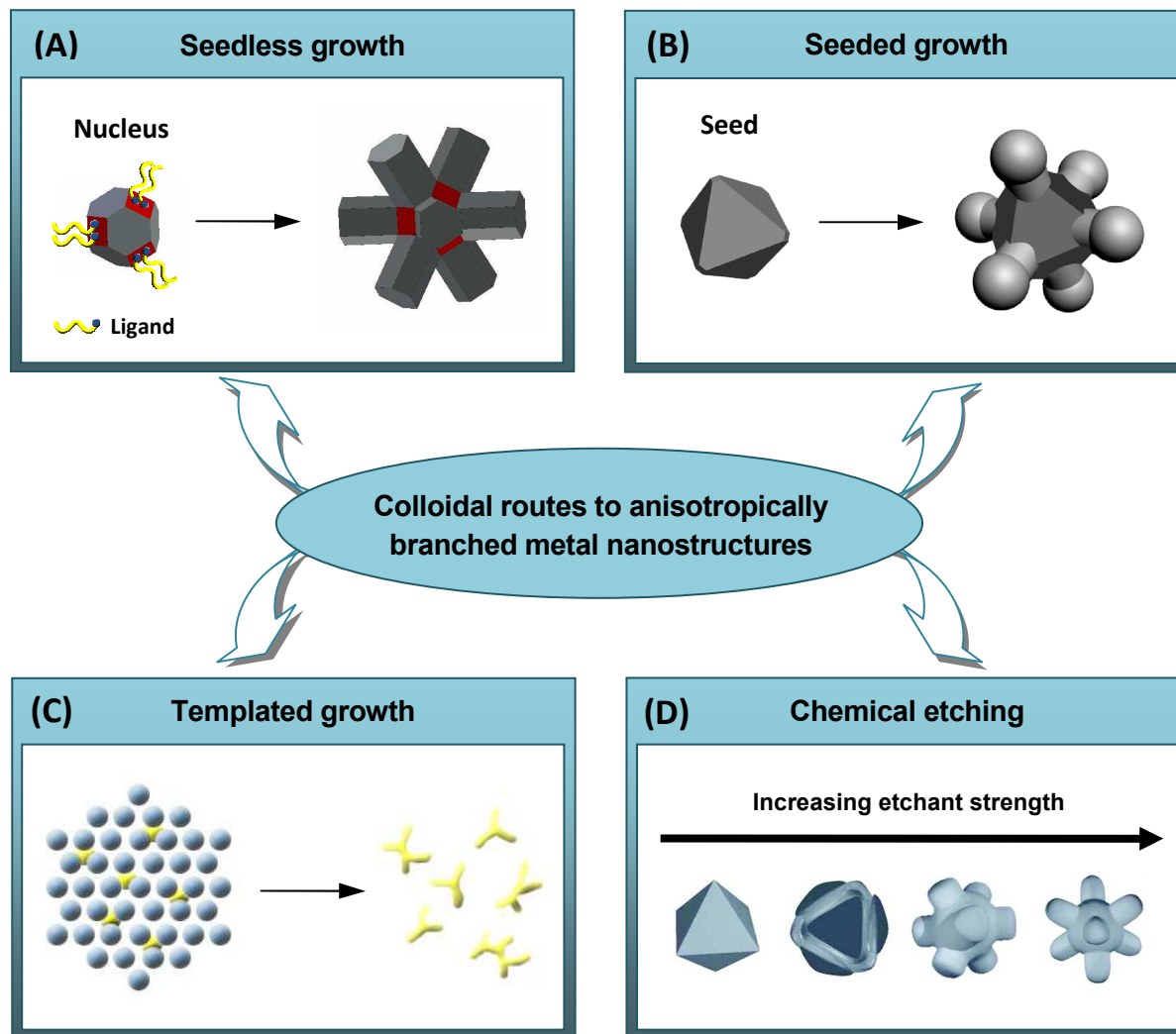


Fig. 1 Colloidal-based strategies for anisotropic branching of metal nanostructures: (A) seedless growth, (B) seeded growth, (C) templated growth, and (D) chemical etching in a controlled manner. (B) is adapted with permission from ref. 29. Copyright 2011 Wiley-VCH. (D) is reproduced with permission from ref. 41. Copyright 2010 American Chemical Society.

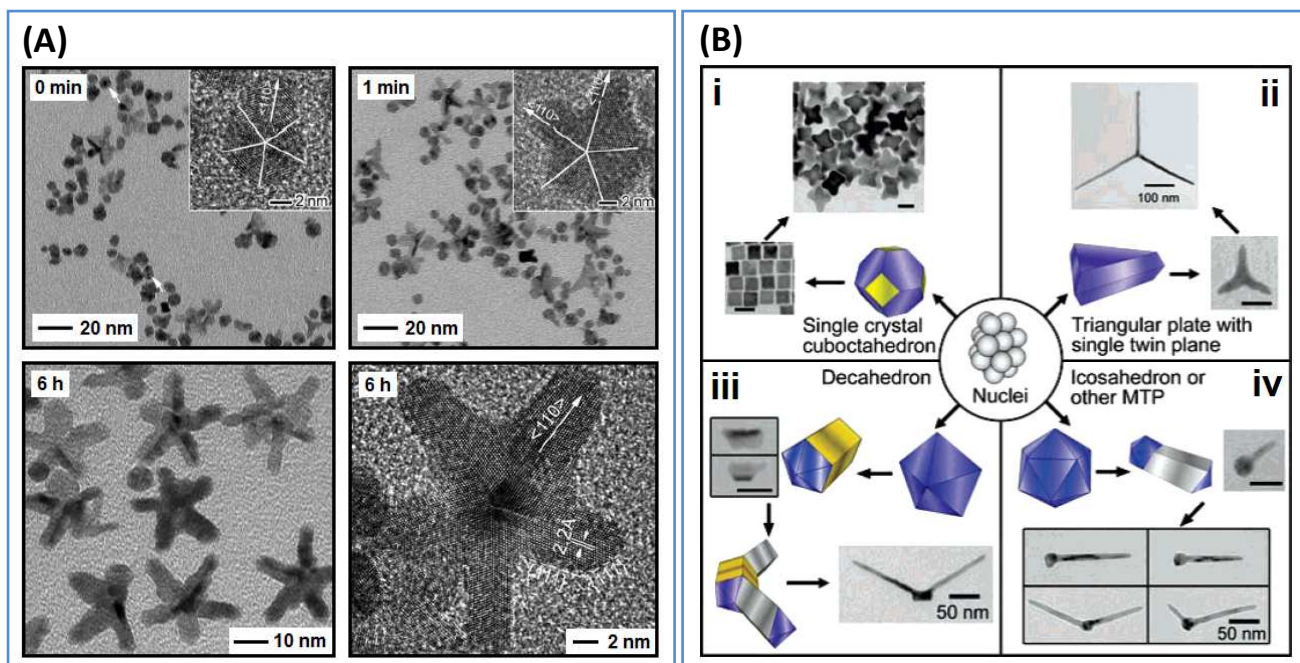


Fig. 2 Twin-determined branching. (A) TEM and HRTEM images of Rh nanocrystals at different reaction times. The multiply-twinned Rh decahedral nanocrystals that form in the initial stage of the reaction (time = 0 min) eventually transform into starfish-like nanostructures (time = 6 h). At time = 1 min, it can be seen that arms start to grow from the five twin boundary corners of the decahedron along the $\langle 110 \rangle$ direction. Adapted with permission from ref. 14. Copyright 2010 Wiley-VCH. (B) Schematic illustration that shows the evolution of Pt nuclei to branched nanostructures. The final morphology is determined by the number of twin planes in the initially formed nanocrystals. Reproduced with permission from ref. 15. Copyright 2007 American Chemical Society.

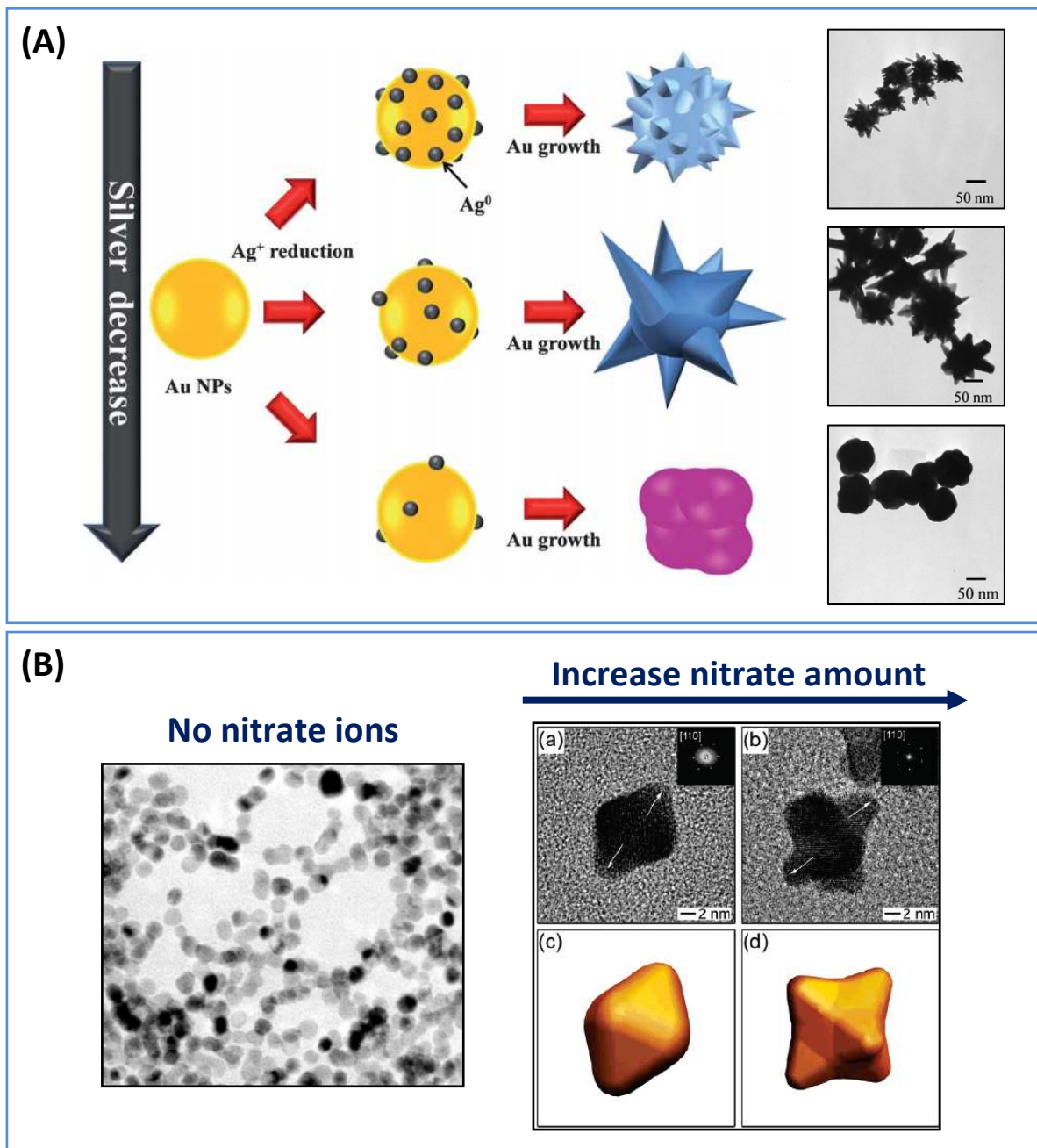


Fig. 3 Ion-induced branching. (A) Schematic illustration of the Ag^+ -mediated growth of branched Au nanocrystals. The size and number of branches can be tuned by varying the Ag^+ concentration. The TEM images of the resulting nanostructures are shown on the right. Adapted from ref. 16. (B) NO_3^- -mediated growth of branched Pt nanocrystals. The TEM image on the left shows the spheroidal Pt nanocrystals that were obtained in the absence of NO_3^- . The effect of increasing the NO_3^- concentration is seen on the

right. The HRTEM images (a, b) and the corresponding models (c, d) show that the growth of Pt nanocrystals was substantially enhanced at ridges and corners to form multipods. Adapted with permission from ref.19. Copyright 2004 American Chemical Society.

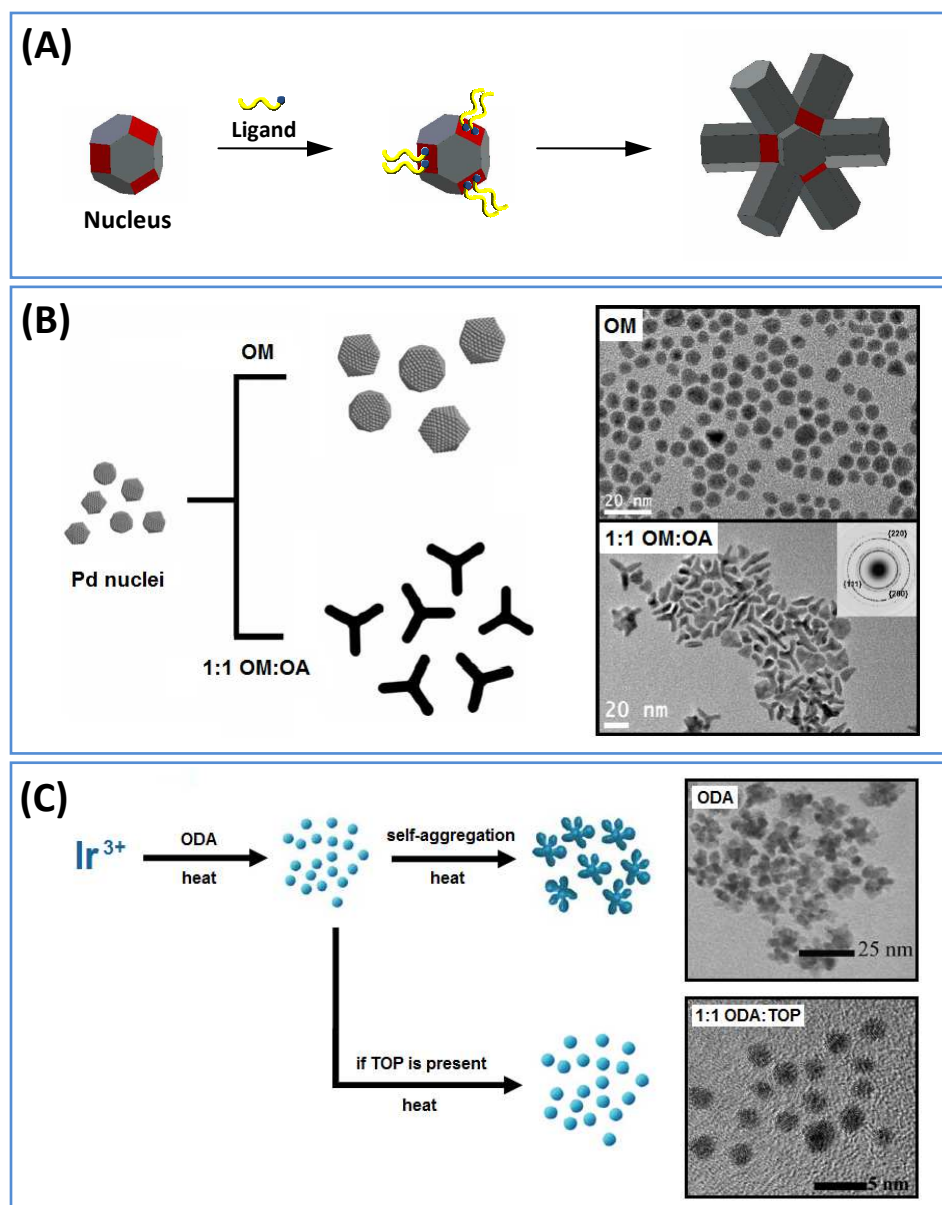


Fig. 4 Ligand-controlled branching. (A) Pictorial representation that shows the ability of ligands to direct the formation of branched nanostructures. The preferential adsorption of the ligand molecules to a particular crystallographic facet slows the growth rate of that

facet relative to others. (B) Schematic depiction and TEM images showing the ligand-dependent shape-controlled synthesis of Pd nanocrystals. The difference in morphology of the resulting Pd nanocrystals is due to the different binding abilities of oleylamine (OM) and oleic acid (OA) to Pd. Adapted with permission from ref. 22. Copyright 2009 Wiley-VCH. (C) Schematic depiction and TEM images showing the ligand-controlled self-aggregation of Ir nanocrystals. Octadecylamine (ODA), a ligand with weak binding affinity toward Ir, promotes the self-aggregation of the weakly passivated Ir nanocrystals into nanodendrites. In the presence of trioctylphosphine (TOP), the growth of well-passivated quasi-spherical nanocrystals is favored. Adapted from ref 25.

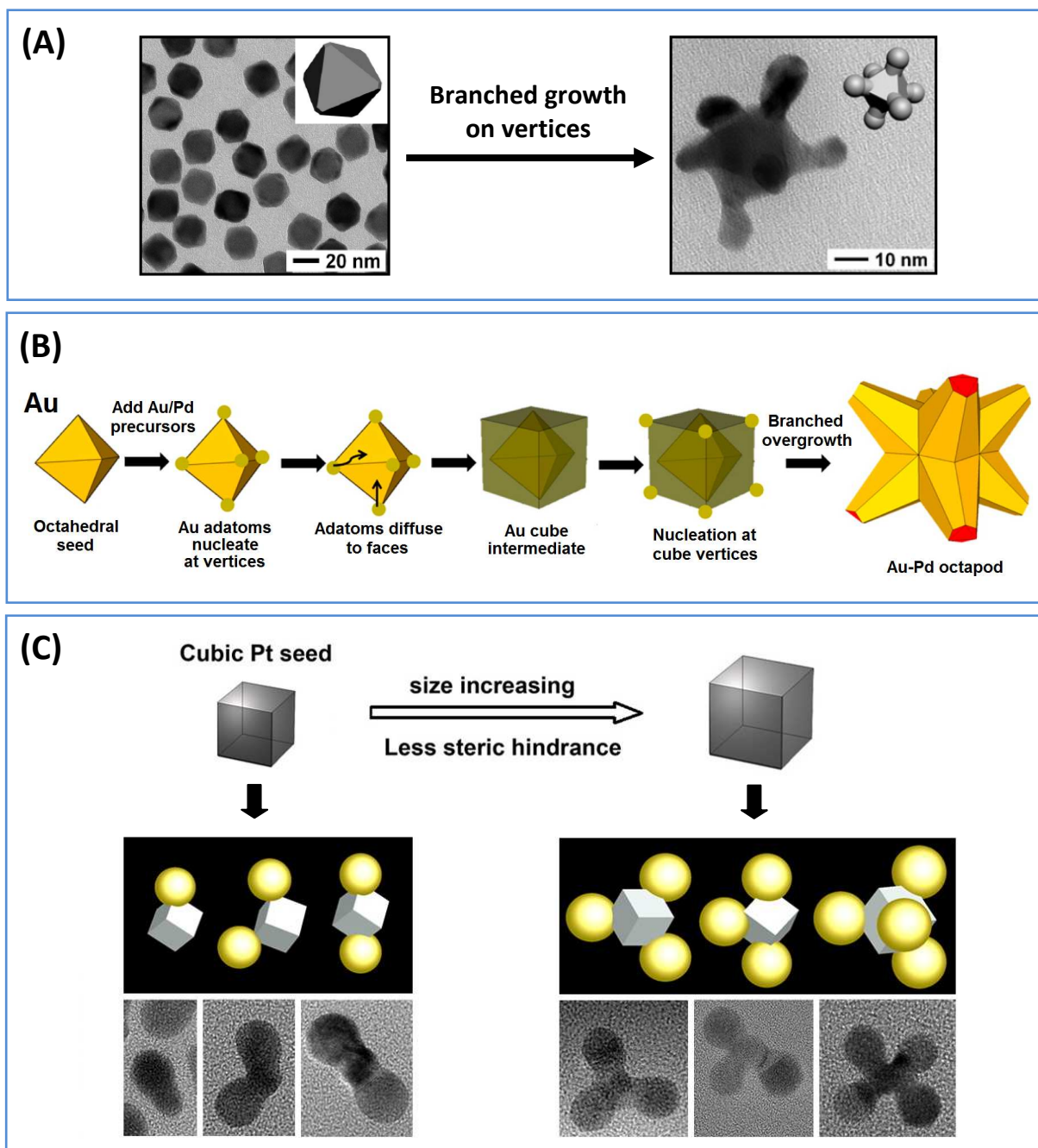


Fig. 5 Seeded growth of branched metal nanostructures. (A) Formation of Au nanohexapods *via* branched growth on the six vertices of octahedral-shaped Au nanocrystal seeds. Adapted with permission from ref. 29. Copyright 2011 Wiley-VCH. (B) Schematic representation that illustrates the formation of Au–Pd nano-octapods from octahedral-shaped Au nanocrystal seeds. The initial Au octahedron restructures to a cubic intermediate prior to branching. Adapted with permission from ref. 32. Copyright 2014

American Chemical Society. (C) Growth of Au branches on the vertices of cubic Pt nanocrystal seeds. The number of branches increases with increasing seed size as a result of reduced steric hindrance. Adapted with permission from ref. 35. Copyright 2014 American Chemical Society.

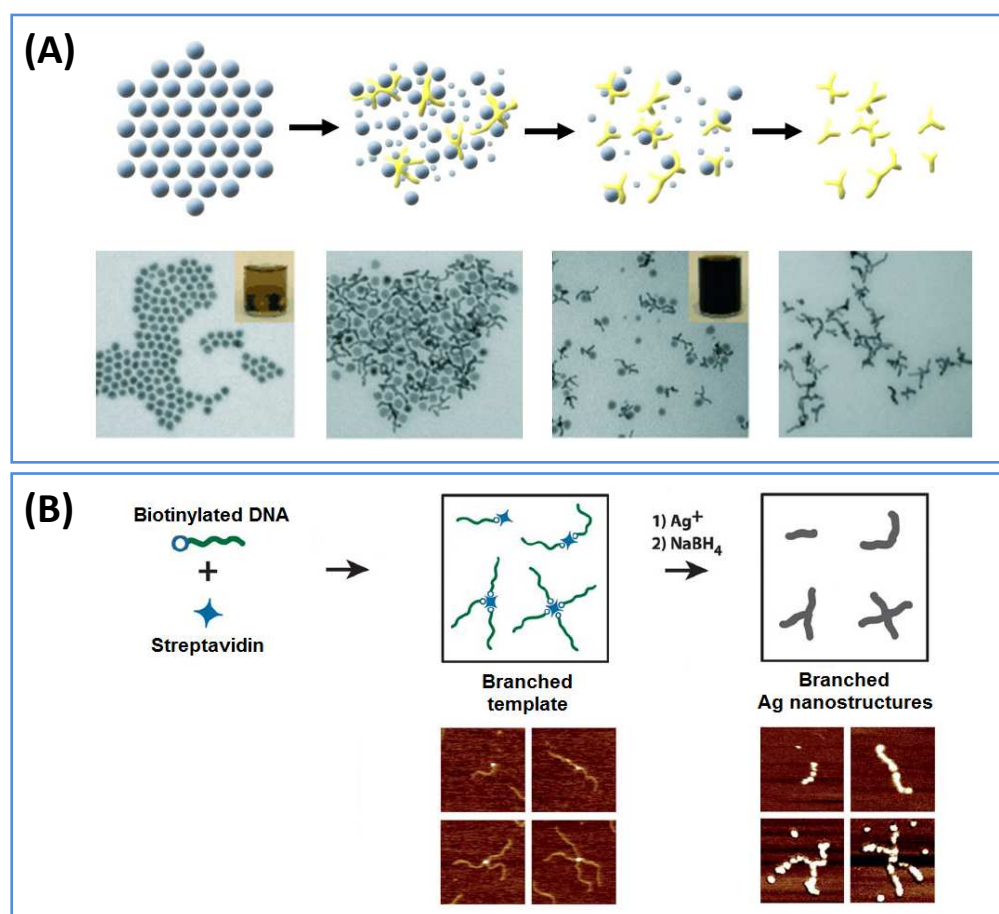


Fig. 6 Templated growth of branched metal nanostructures. (A) Schematic diagram and TEM images showing the formation of branched Au nanostructures using an array of magnetic Fe nanoparticles as template. The Fe nanoparticle array does not only serve as a scaffold, but also participates in the chemical reaction and eventually self-destructs to release the Au multipods. Adapted with permission from ref. 36. Copyright 2008 Wiley VCH. (B) Schematic depiction and AFM images that show the formation of branched Ag nanostructures using a branched template based on DNA-protein assemblies. The branched template is composed of a single streptavidin protein core that is surrounded by one to four biotinylated DNA molecules. Adapted from ref. 39.

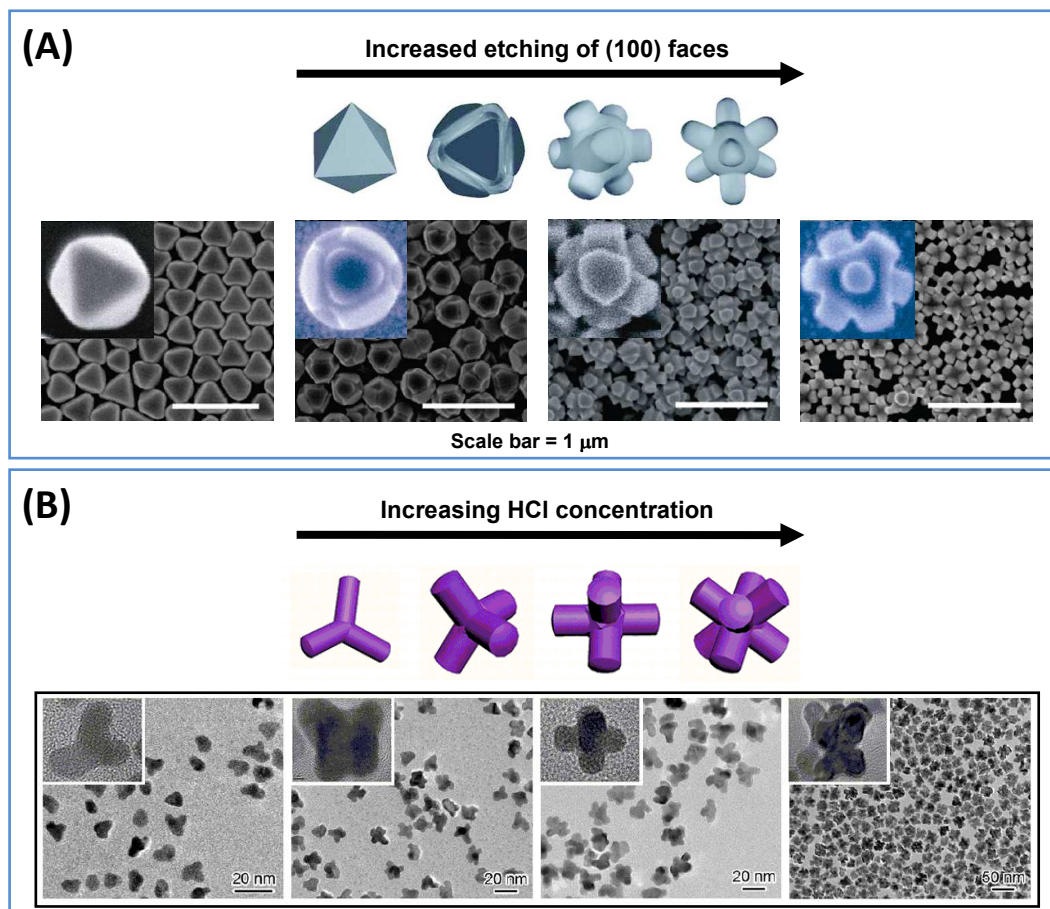


Fig. 7 Chemical etching route to branched metal nanostructures. (A) Schematic depiction and SEM images showing the etching progress of octahedral-shaped Ag nanocrystals using an etchant formulation that preferentially etches in the [100] direction. Adapted with permission from ref. 41. Copyright 2010 American Chemical Society. (B) Schematic depiction and TEM images that show the effect of varying amounts of HCl on the extent of oxidative etching of Pt nanocrystals. Adapted with permission from ref. 42. Copyright 2012 American Chemical Society.

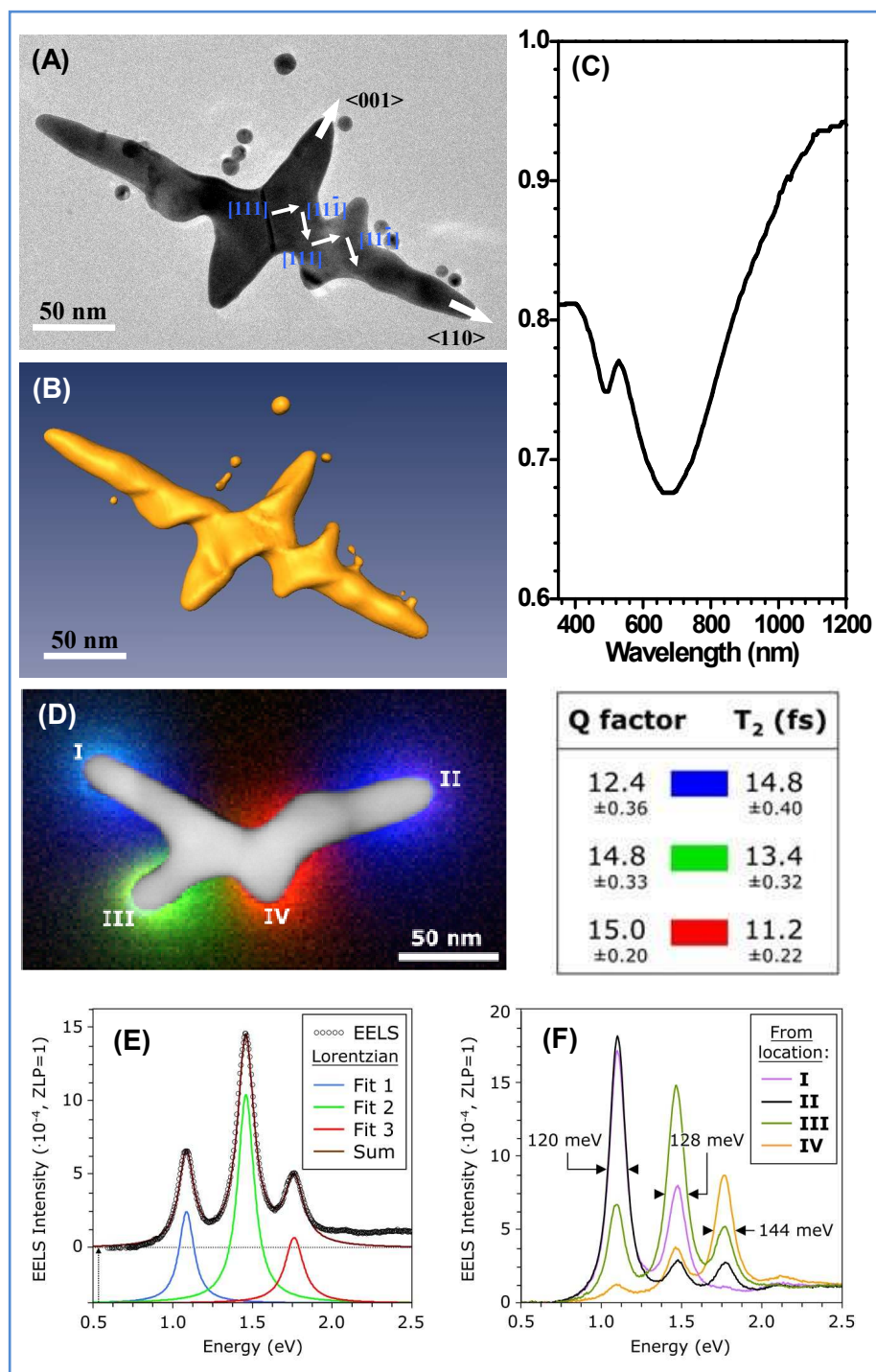


Fig. 8 Plasmonic properties of Au nanocrosses. (A) TEM image and (B) reconstructed HAADF-STEM tomography image of a single Au nanocross. (C) Absorption spectrum of Au nanocrosses. Reproduced with permission from ref. 18. Copyright 2011 American Chemical Society. (D-F) Quantitative mapping of the quality factors Q and dephasing

times T_2 of individual plasmon modes in a single Au nanocross: (D) Overlaid, colour-coded EELS maps from the three dominant plasmon modes. Their Q and T_2 values are provided on the right. (E) EELS spectrum from location III to which three Lorentzians are fitted. (F) EELS spectra from locations I-IV, showing three dominant plasmon modes and their widths, as measured from Lorentzian fitting. Reproduced with permission from Macmillan Publishers Ltd: Nature (ref. 46), Copyright 2013.

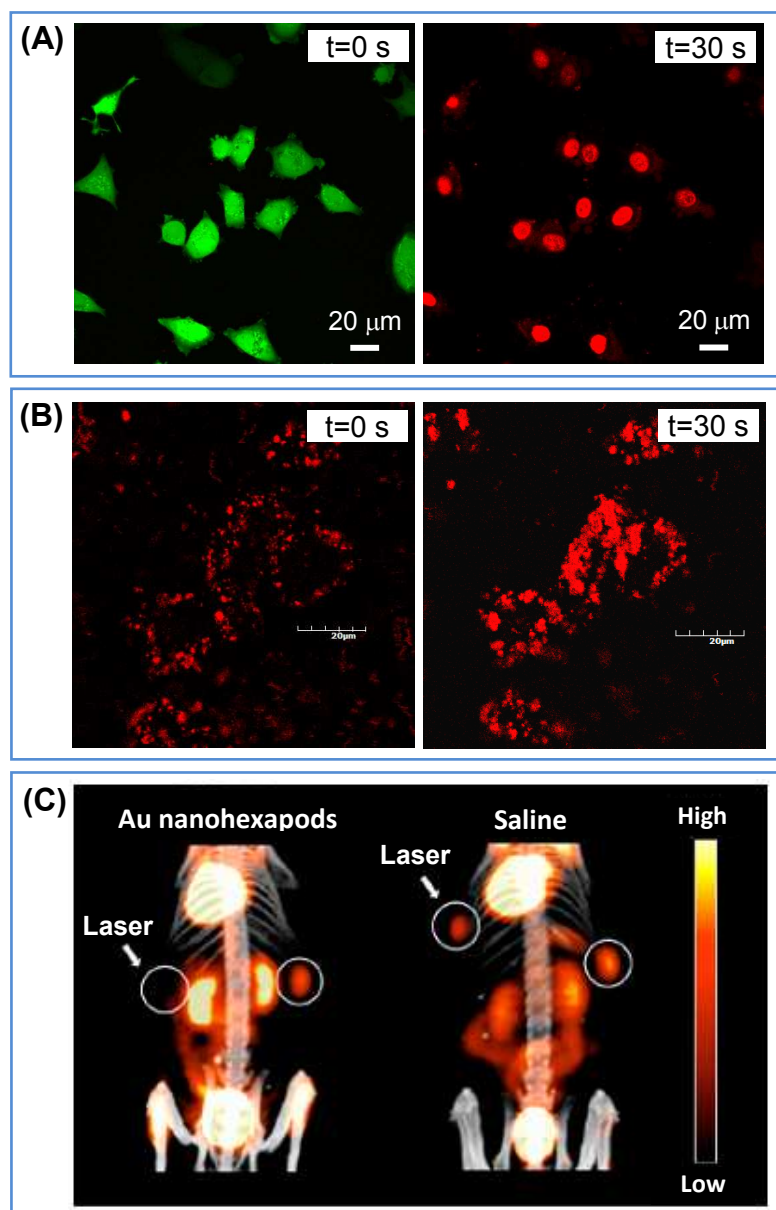


Fig. 9 Biological applications of branched Au nanostructures. (A-B) Effective photothermal destruction of cancer cells associated with Au nanocrosses. (A) Confocal fluorescence images of the cancer cells before 900-nm laser exposure (left) and after

laser irradiation for 30 s (right). The living cells are marked by green fluorescence whereas the dead cells are indicated by red fluorescence. (B) Two-photon luminescence images of the Au nanocrosses associated with cells before 900-nm laser exposure (left) and after laser irradiation for 30 s (right). Reproduced with permission from ref. 18. Copyright 2011 American Chemical Society. (C) ^{18}F -FDG PET/CT co-registered images of mice intravenously administrated with an aqueous suspension of Au nanoheptapods and saline solution. Tumor locations are marked with white circles. Irradiated tumors are highlighted with white arrows. Reproduced with permission from ref. 48. Copyright 2013 American Chemical Society.

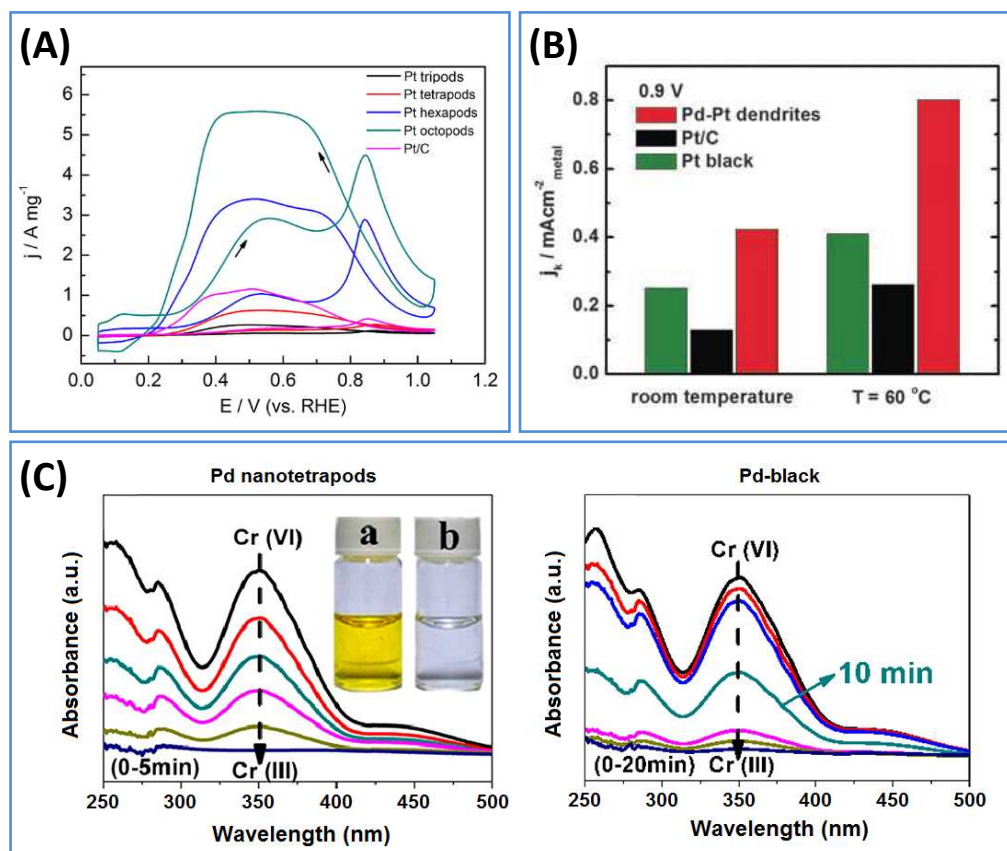


Fig. 10 Catalytic applications of branched metal nanostructures. (A) Cyclic voltammograms (mass activities) of branched Pt nanostructures and Pt/C catalyst (Electrolyte: 0.5 M H_2SO_4 + 0.1 M HCOOH solution; scan rate, 50 mV/s). The catalytic activity for formic acid oxidation increases with increasing number of branches. Reproduced with permission from ref. 42. Copyright 2012 American Chemical Society. (B) Specific activities for ORR (at 0.9 V vs. RHE) of different Pt-based catalysts. The

Pd–Pt nanodendrites outperformed the commercial Pt/C and Pt-black catalysts.

Reproduced with permission from ref. 49. Copyright 2009, AAAS. (C) Temporal evolution of the absorption spectra associated with the reduction of $\text{Cr}_2\text{O}_7^{2-}$ with formic acid at 50 °C in the presence of Pd nanotetrapods (left) and commercial Pd-black (right).
Reproduced with permission from ref. 20. Copyright 2014 American Chemical Society.